

SUPERLUMINOUS SPIRAL GALAXIES

PATRICK M. OGLE¹, LAURANNE LANZ¹, CYRIL NADER^{1,2}, GEORGE HELOU¹¹IPAC, California Institute of Technology, Mail Code 220-6, Pasadena, CA 91125 and²University of California, Los Angeles*Draft version September 25, 2017*

ABSTRACT

We report the discovery of spiral galaxies that are as optically luminous as elliptical brightest cluster galaxies, with r-band monochromatic luminosity $L_r = 8 - 14L_*$ ($4.3 - 7.5 \times 10^{44}$ erg s⁻¹). These super spiral galaxies are also giant and massive, with diameter $D = 57 - 134$ kpc and stellar mass $M_{stars} = 0.3 - 3.4 \times 10^{11} M_\odot$. We find 53 super spirals out of a complete sample of 1,616 SDSS galaxies with redshift $z < 0.3$ and $L_r > 8L_*$. The closest example is found at $z = 0.089$. We use existing photometry to estimate their stellar masses and star formation rates (SFRs). The SDSS and WISE colors are consistent with normal star-forming spirals on the blue sequence. However, the extreme masses and rapid SFRs of $5 - 65 M_\odot \text{ yr}^{-1}$ place super spirals in a sparsely populated region of parameter space, above the star-forming main sequence of disk galaxies. Super spirals occupy a diverse range of environments, from isolation to cluster centers. We find four super spiral galaxy systems that are late-stage major mergers—a possible clue to their formation. We suggest that super spirals are a remnant population of unquenched, massive disk galaxies. They may eventually become massive lenticular galaxies after they are cut off from their gas supply and their disks fade.

1. INTRODUCTION

The most massive galaxies in the universe are thought to form from the largest density peaks in the primordial matter distribution. Galaxy mergers change the initial galaxy mass function, forming more massive galaxies by combining less massive ones. The result is the galaxy mass distribution we see in the local universe, empirically described by the Schechter (1976) luminosity function, together with a morphology-dependent mass-to-light ratio. The luminosity function also depends upon the star formation history of galaxies, regulated by gas content, gas accretion, stellar feedback, and active galactic nucleus (AGN) feedback. Galaxy mergers play an important role here too, since tidal torques in merging systems tend to force gas into the galaxy centers, increasing the surface density of molecular gas and leading to starburst and AGN activity (Toomre & Toomre 1972; Barnes & Hernquist 1991).

Galaxies segregate into two major classes based on color and morphology (Strateva et al. 2001; Lintott et al. 2008). Blue, star-forming disks (late-type galaxies, LTGs) lie in one region of color-space called the blue-sequence. Red-and-dead ellipticals (early-type galaxies, ETGs) lie in a different region of color space called the red sequence. LTGs demonstrate a correlation between star formation rate (SFR) and stellar mass (M_{stars}) called the star-forming main sequence (SFMS). The SFMS may be a consequence of an equilibrium between inflowing gas and star-formation driven outflows, with the specific star formation rate (SSFR) regulated by the halo mass growth rate (Lilly et al. 2013). Most ETGs on the other hand have much lower star formation rates because they lack the cold gas needed to sustain star formation. It appears that there is a limit to the mass of star-forming disk galaxies of roughly $3 \times 10^{10} M_\odot$, with the most massive disk galaxies

slowly transitioning away from the main sequence as their SSFR declines. This decline appears to be a gradual process, occurring over a period longer than 1 Gyr after the gas supply to the galaxy disk has been interrupted (Schawinski et al. 2014). Rapid quenching does not appear to occur for most galaxies that remain disk galaxies, contrary to early attempts to explain the apparently bimodal distribution of galaxy colors.

A number of mechanisms have been suggested to explain why the gas supply is interrupted for the most massive disk galaxies. Major galaxy mergers may disrupt merging disk galaxies and transform them rapidly into elliptical galaxies (Baldry et al. 2004), though this does not explain the transformation of galaxies that remain disks. The accretion of cold gas onto a galaxy may be stopped when the galaxy halo becomes massive enough that accretion shocks develop, interrupting the cold streams of gas needed to replenish the disk (Dekel & Birnboim 2006). Increasing AGN feedback from a growing supermassive black hole may shock or eject gas from the galaxy disk, reducing its capacity to form stars (Hopkins et al. 2006; Ogle, Lanz, & Appleton 2014). Ram-pressure stripping of the interstellar medium (ISM) by the intercluster medium (ICM) of a galaxy cluster can also remove cold gas (Sivanandam, Rieke, & Rieke 2014).

Studying the most massive spiral galaxies can give us clues as to which of the above evolutionary processes are primarily responsible for converting star-forming disk galaxies into red-and-dead lenticulars or ellipticals. The existence of rapidly star-forming, massive spirals with $M_{stars} > 10^{11} M_\odot$ indicates that disk galaxies can postpone this fate under special circumstances.

We present here the most optically luminous and biggest spiral galaxies in the local universe, found by mining the NASA/IPAC Extragalactic Database (NED). We assume a cosmology with $H_0 = 70$, $\Omega_m = 0.3$, and $\Omega_\Lambda = 0.7$ for computing all linear sizes and luminosities.

2. SAMPLE

This project is an offshoot of our work to determine the completeness of NED and explore its potential for systematic studies of galaxy populations (Ogle et al., in preparation). NED provides a unique fusion of multi-wavelength photometry from Galaxy Evolution Explorer (GALEX), Sloan Digital Sky Survey (SDSS), and the 2-Micron All-Sky Survey (2MASS), among others, which we augment by Wide-field Infrared Survey Explorer (WISE) photometry, that allows us to estimate stellar masses and star formation rates. We compared the redshift distribution of galaxies in NED at $z < 0.3$ to a model redshift distribution for the universe derived using a redshift-independent luminosity function, in order to estimate the spectroscopic completeness of NED. We used the Schechter (1976) luminosity function fits of Blanton et al. (2003), which are based on $\sim 150,000$ SDSS galaxies as our benchmark. We adopt their characteristic absolute magnitude value of $M^* - 5 \log_{10} h = -20.44 \pm 0.01$ ($L^* = 5.41 \times 10^{43} \text{ erg s}^{-1}$ at 6200 \AA) for the SDSS r-band luminosity function. The redshift limit was made large enough to capture the rarest, most luminous galaxies, but not so large as to require consideration of redshift evolution in the luminosity function.

2.1. SDSS r-band Selection of the most Optically Luminous Galaxies

SDSS is the largest source of spectroscopic redshifts, with a spectroscopic selection limit of $r=17.77$ (Strauss et al. 2002). We find that NED is complete over the SDSS footprint out to $z = 0.3$ for galaxies with $L_r > 8L^*$, the most optically luminous and massive galaxies in the local universe. Our sample is chosen from the 797,729 galaxies (type=G) in NED with spectroscopic redshifts $z < 0.3$, in the SDSS footprint, and detected in SDSS r band. We apply Galactic extinction corrections (tabulated by NED) and K-corrections to the r-band magnitudes prior to making our sample selection. We find 1,616 galaxies with redshift $z < 0.3$ and luminosity $L_r > 8L^*$, which constitute our Ogle et al. Galaxy Catalog (OGC). The most luminous galaxy in the OGC is a $20L^*$ elliptical brightest cluster galaxy (BCG).

2.2. UV Selection Method for Super Spiral Galaxies

We make a further selection for UV emission because we are interested in finding the most massive, actively star-forming disk galaxies. We recently matched and integrated the GALEX All-Sky Survey Catalog (GASC) and GALEX Medium Sky Survey Catalog (GMSC) with NED, using an automated, statistical algorithm (Ogle et al. 2015). We inspected the SDSS images of all 196 galaxies from the OGC that are detected in the GALEX NUV band (the OGC-UV subsample). Of these, we find 46 NUV-detected, $L_r > 8L^*$ galaxies with spiral morphology (Table 1). The remaining NUV sources include 118 ellipticals, 11 galaxies with E+A spectra, 2 quasi-stellar objects (QSOs) with extended emission, and 19 galaxies with erroneous redshifts or magnitudes. The most luminous elliptical galaxy in OGC-UV is a $16L^*$ BCG, while the most luminous spiral galaxy has $L_r = 14L^*$.

2.3. Morphological Selection Method for Super Spiral Galaxies

We inspected the 310 brightest galaxies of the full OGC sample, those with $L_r > 10.5L^*$, to see if we are missing any spirals with UV selection. Of these, we classified 11 super spirals, 253 ellipticals, 38 galaxies with erroneous redshifts or magnitudes, 6 lenticulars, 1 irregular, and 1 E+A galaxy. This inventory includes 7 additional super spirals (Table 1) that are not in the OGC-UV sample. Of these, 4 have no GALEX sources nearby, and 3 others have nearby GALEX sources that should be matched in NED, but are not, possibly because of confusion. This shows that our NUV selection, while relatively efficient (47/196) compared to morphological selection (11/310), leads to an incomplete sample, with only 4/11 super spirals recovered in this luminosity range. Part of the incompleteness (3/11) is owing to incomplete matching of GALEX with NED, while the rest (4/11) may be attributed to the GALEX detection limit or coverage.

3. PHOTOMETRY

We conduct our investigation of super spirals primarily with photometry compiled by NED. We use SDSS DR6 u, g, r, i, z photometry measured with the CModel method, which combines exponential plus deVaucouleurs model fitting. GALEX FUV and NUV photometry is taken from the GASC and GMSC, measured within a Kron elliptical aperture. We use 2MASS J, H, Ks total magnitudes from the 2MASS Extended Source Catalog (2MASX). NED objects are matched to WISE using the Gator tool in the Infrared Science Archive (IRSA). We use AllWISE [4.6] and [12] μm photometry within the largest available fixed-radius aperture of $24''.75$, which is well-matched to the largest galaxy in our sample, with semi-major axis $a = 24''.5$.

4. BASIC PROPERTIES OF SUPER SPIRALS

4.1. Optical and Mid-IR colors

The SDSS and WISE colors of super spirals lie along the blue sequence, similarly to less luminous star-forming disk galaxies (Figure 1a). The SDSS comparison sample is adopted from Alatalo et al. (2014), who show that LTGs and ETGs classified by Galaxy Zoo (Lintott et al. 2008) are well-separated in WISE [4.6]-[12] vs. SDSS u-r color space. The WISE [4.6] - [12] color ranges from 2.0-4.2, typical of polycyclic aromatic hydrocarbon (PAH) and warm dust emission from gas-rich, actively star-forming galaxies. The u-r color ranges from 1.4-4.4, indicating star-forming disks with a range of SSFR. We estimate differential K-corrections of $\Delta(u-r) < 0.2 \text{ mag}$ in the redshift range $z = 0.1 - 0.3$, by convolving several spectral energy distribution (SED) models (e.g., those in the Appendix) with the SDSS filter curves. These corrections are not large enough to explain the additional scatter in the observed u-r colors of super spirals.

There is a shift in the locus of super spiral colors compared to less-massive blue sequence galaxies. Super spirals tend to have redder u-r and bluer [4.6]-[12] colors compared to the SDSS distribution. This could in principle indicate either lower SSFR or increased extinction. However, the high SSFR of our sample (Fig 1b) runs contrary to the first explanation. Six super spirals have $u-r > 3.0$, a value not attained by normal SDSS

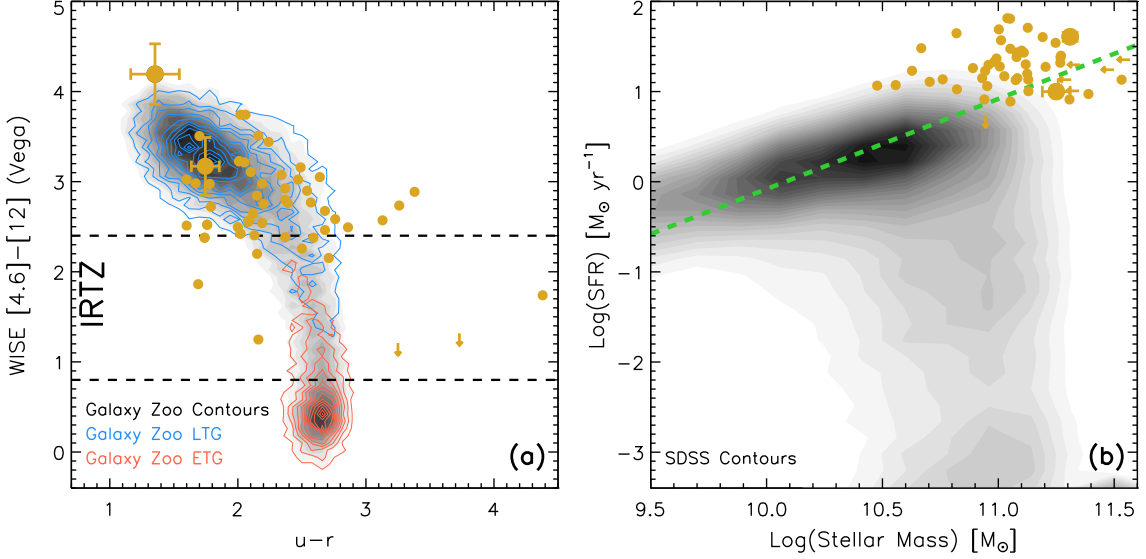


Figure 1. (a) SDSS and WISE colors of super spirals (filled circles) compared to other SDSS galaxies classified as LTG or ETG by Lintott et al. (2008). The infrared transition zone (IRTZ) is the mid-IR equivalent of the optical green valley (Alatalo et al. 2014). (b) Star formation rates and stellar masses of super spirals compared to the SDSS-WISE sample of Chang et al. (2015). The dashed line indicates a formation time of 12 Gyr at $z = 0.1$. Galaxies above this line have formation times less than the age of the universe. Larger symbols are for SDSS J094700.08+254045.7 and 2MASX J13275756+334529, with detailed SED analysis presented in the Appendix.

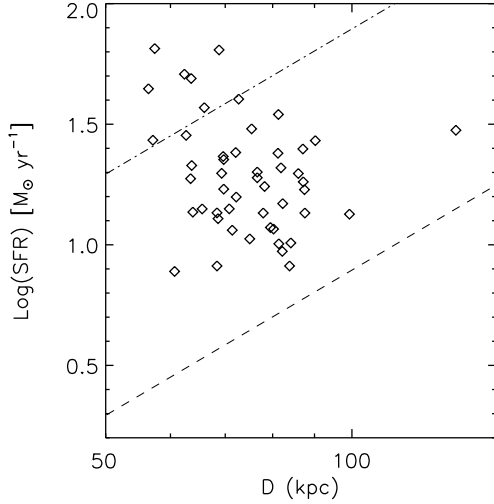


Figure 2. Super spirals range in diameter from 57-134 kpc. The dashed and dot-dashed lines indicate deprojected SFR surface densities of 1×10^{-3} and $1 \times 10^{-2} M_{\odot} \text{ yr}^{-1} \text{ kpc}^{-2}$, respectively.

late-type galaxies. The two reddest galaxies (2MASX J00380781-0109365 and 2MASX J09094480+2226078) may be misclassified peculiar elliptical galaxies with prominent shells. CGCG 122-067 may be redder because of its double bulge. The other 3 are clearly spirals, and require further investigation and custom photometry to determine the cause of their unusually red $u-r$ colors.

4.2. Stellar Mass and Star Formation Rate

We estimate stellar mass from 2MASS Ks luminosity together with an SDSS $u-r$ color-dependent mass-to-light ratio estimated using the prescription of Bell et al. (2003), giving $M/L = 0.75 - 1.34 M_{\odot}/L_{\odot}$. This yields stellar masses that are consistent with more sophisticated SED template fitting (Appendix). We find stellar masses

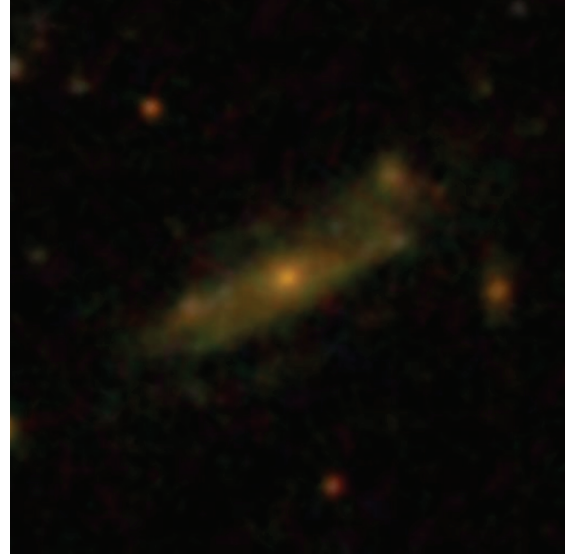


Figure 3. The largest super spiral galaxy, with $L_r = 12L_{*}$ and an isophotal diameter of 134 kpc, 2MASX J16394598+4609058 ($z = 0.24713$). The SDSS image is $50.7''$ (197 kpc) on each side.

in the range $M = 0.3 - 3.4 \times 10^{11} M_{\odot}$.

We estimate the SFR from the WISE [12] micron luminosity using the prescription of Chang et al. (2015), which was established by SED-fitting more than 630,000 SDSS galaxies with MAGPHYS (da Cunha, Charlot, & Elbaz 2008). While accurate for star-forming galaxies, this method may overestimate the star-formation rate for early type galaxies where dust may be heated by other sources not directly related to star formation, or in the presence of a luminous AGN. We further validate our WISE single-band SFRs against MAGPHYS SED-fitting for two representative super spirals (Appendix). The WISE [12] monochromatic luminosities of super spirals range from $0.3 - 3.5 \times 10^{44} \text{ erg s}^{-1}$ ($0.8 - 9.8 \times 10^{10} L_{\odot}$), corresponding to SFRs of

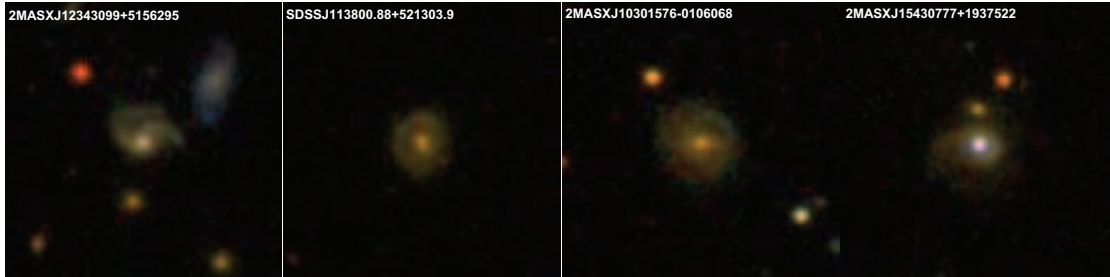


Figure 4. SDSS images of super spirals with peculiar morphology. (a) Asymmetric 2-arm spiral. (b) Ring galaxy. (c) Multi-arm spiral. (d) QSO host with tidal arm. Each SDSS image is $48''$ on a side.



Figure 5. SDSS images of super spiral merger candidates. (a) Possible collision in progress of two spirals. (b) Possible collision or merger of two spirals, also a brightest cluster galaxy (Figure 6). (c) High-surface brightness disk with possible double AGN, with faint outer arms. The nucleus at the center is classified as an SDSS QSO. The second bright point source and possible AGN, near the edge of the disk, has a similar color to the primary AGN. (d) Possible late-stage major merger with two stellar bulges, with a striking grand spiral design surrounding both nuclei. Three other point sources may mark additional merging components or nuclei, reminiscent of nest galaxies commonly found at the centers of galaxy clusters. Each SDSS image is $48''$ on a side.

$5 - 65 M_{\odot} \text{ yr}^{-1}$.

We compare our sample to the SDSS-WISE sample of Chang et al. (2015), who estimated SFR and M_{stars} with MAGPHYS. We find that most super spirals lie well above an extrapolation of the star-forming main sequence to higher mass (Figure 1b). This is a region of the SFR vs. mass diagram that is very sparsely populated. The vast majority of SDSS disk galaxies in this mass range have significantly lower SFR and SSFR.

Our r-band luminosity plus NUV detection criteria tend to select galaxies with high global star formation rates. However, the SDSS spectra reveal a relatively old bulge stellar population for most super spirals. We do find an indication of starburst activity in the SDSS bulge spectra of 3 super spirals (2MASX J13275756+3345291—see Appendix, 2MASX J1003568+382901, and 2MASX J10041606+2958441) with strong young stellar population contributions and high-equivalent width H α emission. These three galaxies also have relatively blue SDSS u-r colors and red WISE [4.6]-[12] colors, both indicative of a high global SSFR.

4.3. Active Galactic Nuclei

There are 3 Seyfert 1 nuclei and 2 QSOs with broad Balmer lines and strong [O III] in their SDSS spectra (Table 1). There is also 1 Seyfert 2 nucleus with strong [O III] but narrow Balmer lines. There is likely a dominant contribution from the QSO to the IR luminosity

of 2MASX J15430777+1937522, which has the greatest WISE [12] luminosity of the sample ($1.7 \times 10^{45} \text{ erg s}^{-1}$ or $4.3 \times 10^{11} L_{\odot}$). The presence of luminous AGNs in 11% of super spirals indicates that they are continuing to grow their supermassive black holes. It is imperative to measure the distribution of bulge and supermassive black hole masses in our super spiral sample to see if they follow the same relation as lower-mass spiral bulges.

4.4. Size, SFR Surface Density, and Morphology

The sizes of super spirals range from 57-134 kpc, with a median size of 72 kpc, using the SDSS DR6 r-band isophotal diameter at 25.0 mag arcsec $^{-2}$ (Table 1 and Figure 2). Their deprojected SFR surface densities range from $1.5 \times 10^{-3} - 2.0 \times 10^{-2} M_{\odot} \text{ yr}^{-1} \text{ kpc}^{-2}$. A plot of SFR vs. diameter shows considerable scatter. However, the five most rapidly star forming galaxies, with $\log(\text{SFR}) > 1.6$ all have diameters $D < 70$ kpc. The most MIR-luminous super spiral (SDSS J094700.08+254045.7, see Appendix), also has the largest deprojected SFR surface density. The largest super spiral, 2MASX J16394598+4609058 (Figure 3), has a diameter of 134 kpc and a relatively low SFR surface density of $2.0 \times 10^{-3} M_{\odot} \text{ yr}^{-1} \text{ kpc}^{-2}$.

Super spirals display a range of morphologies, from flocculent to grand-design spiral patterns. At least 9 super spirals have prominent stellar bars visible in SDSS images (Table 1: Notes). There is evidence for morpho-



Figure 6. Super spiral merger candidate 2MASXJ16014061+2718161 is the brightest cluster galaxy of galaxy cluster GMBCG J240.41924+27.30444. The SDSS image is $203''$ (572 kpc) on each side.

logical peculiarities in several cases, including one-arm spirals, multi-arm spirals, rings, and asymmetric spiral structure (Figure 4 and Table 1). These types of features may indicate past or ongoing galaxy mergers or collisions.

5. GALAXY MERGER CANDIDATES

We find four super spiral merger candidates with apparent double stellar bulges or double nuclei (Figure 5). The SDSS spectra only cover the dominant or central bulge or nucleus of each system. Spectroscopy of the secondary bulges or nuclei will be necessary to confirm or rule out these merger candidates as true physical pairs or multiples.

The merger candidate 2MASX J08542169+0449308 appears to be a nearly equal mass major spiral pre-merger. The arms of both spirals are wound in the same direction, and the disks appear to be overlapping in the plane of the sky. The stretched out spiral arms of both spiral galaxy components, together with an ap-

parent tidal arm at $PA = 0^\circ$ (measured counterclockwise from North) suggest an ongoing tidal interaction.

The merger candidate 2MASX J16014061+2718161 is a brightest cluster galaxy, surrounded by several other disk galaxy companions (Figures 5 and 6). The host cluster is identified as GMBCG J240.41924+27.30444, with a photometric redshift of 0.193 (Table 2). There are clear distortions to the spiral structures of both spiral galaxy components that appear to be involved in this merger.

The merger candidate 2MASX J09334777+2114362 appears to be a double AGN system. The primary, central nucleus is identified as an SDSS QSO. The secondary nucleus has similar flux and color to the primary nucleus, but it does not have an SDSS spectrum to confirm that it is a true physical double AGN. The galaxy disk has high surface brightness, suggestive of starburst activity. Faint outer spiral arms are also suggestive of a recent galaxy interaction.

The merger candidate and brightest cluster galaxy



Figure 7. Super spiral 2MASX J11535621+4923562 ($L_r = 9.5L_*$, $D = 90$ kpc) appears to be the brightest member of a previously unidentified galaxy cluster (OGC 0586 CLUSTER). Compare to the less-luminous cluster spiral galaxy SDSS J115407.96+492200.8 ($L_r = 2.8L_*$, $D = 39$ kpc) in the lower left corner. The SDSS image is $203''$ (579 kpc) on each side.

CGCG 122-067 appears to be a late stage $\sim 2:1$ major merger. The double bulge is surrounded by a common inner disk. Two giant spiral arms emerge from this central disk, one from each bulge, making a complete circuit around the disk. A large gap is seen between the arms at $PA = 0 - 90^\circ$. There are three other possible merging nuclei, including a bright green point source at $PA = 270^\circ$, that raise the possibility that this is a 5-component multiple merger system. Such multiple mergers are reminiscent of the elliptical nest galaxies that are sometimes found at the centers of galaxy clusters. However in the case of gas-rich super spiral BCGs, the merger components may settle into the plane of the disk before migrating to the center of the system through dynamical friction.

6. ENVIRONMENT

We checked NED for known galaxy clusters and groups within $1'$ of each super spiral (Table 2). Seven of the

super spirals are candidate BCGs, within $0.8''$ of a catalogued galaxy cluster. Two are candidate brightest group galaxies (BGGs), within $4''$ of a catalogued galaxy group. Most of the clusters only have photometric redshifts and have yet to be verified spectroscopically. However, the photometric redshifts are all within $\Delta z = 0.04$ of the super spiral spectroscopic redshift, which suggests a true physical association, unless the matching cluster or group redshift is based only on the redshift of the super spiral.

We used NED's Environment Tool to further explore the environments of the super spiral BCG and BGG candidates. This tool performs a redshift-constrained cone search for galaxies and galaxy clusters within a sphere of comoving radius 10 Mpc. Because of the high redshifts of the super spirals, only the most luminous galaxies in their neighborhoods will tend to have measured spectroscopic redshifts in NED. We tabulate the number of galaxies (N1) with spectroscopic redshifts that are within 1 Mpc and 500 km s^{-1} , and the number (N10) within 10 pro-

jected Mpc and 5000 km s^{-1} . The MSPM 05544 galaxy cluster, which appears to host the super spiral CGCG 122-067 has the largest number of cluster members with spectroscopic redshifts in NED (302), while the SDSS-CGB 49074 galaxy group has the smallest number (2). These numbers should be taken as lower limits to the cluster membership, depending primarily on the SDSS spectroscopic selection limit and redshift.

There are likely more clusters to be discovered in the vicinity of super spirals. For example, a clear overdensity of galaxies is seen to the SE of 2MASX J11535621+4923562 (Figure 7). We verify a concentration of 69 galaxies within 10 Mpc and 5000 km s^{-1} (Table 2: OGC 0586 CLUSTER), using NED’s Environment tool.

7. DISCUSSION

While super spirals have similarities to less luminous spiral galaxies, they are unique in the vastness of their scale. A sense of how truly enormous these galaxies are can be gained by comparison to other galaxies in the same cluster (Figure 7: OGC 0586 CLUSTER). The 2MASX J11535621+4923562 super spiral at $z = 0.16673$, with a luminosity of $L_r = 9.5L_*$ and a diameter of 90 kpc, can be compared to a more common, less luminous spiral galaxy which has $L_r = 2.8L_*$ and a diameter of 39 kpc ($13''7$), at about the same redshift ($z = 0.16721$).

7.1. Nearby Analog?

It is natural to ask whether any analogs to super spirals have been found at lower redshift. One well-known example of a large disk galaxy is Malin 1 ($z = 0.083$), initially suggested to be a proto-disk galaxy because of its massive H I disk (Bothun et al. 1987). While Malin 1 does have a large stellar disk with an exponential scale length of 70 kpc, its global r-band luminosity ($L_r = 1.8L_*$) is not nearly great enough to make it into the OGC catalog. Its disk has very low surface brightness and is not readily visible in SDSS images. As further points of comparison, we estimate a global stellar mass of $1.2 \times 10^{10} M_\odot$ and global SFR of $1.2 M_\odot \text{ yr}^{-1}$, which are both much lower than the range spanned by super spirals.

7.2. Formation and Survival

Because super spirals are so rare in the universe, with an average number density of only 32 Gpc^{-3} at $z < 0.3$, it is necessary to survey a very large volume to find one. Even the largest galaxy evolution simulations to date, such as the Illustris simulation (Vogelsberger et al. 2014; Snyder et al. 2015), covering $\sim 1.0 \times 10^{-3} \text{ Gpc}^3$, are not big enough to manufacture a significant number of super spirals. Therefore, no adequate prediction exists for the expected number of super spirals at $z < 0.3$, nor are there simulations showing how these giant galaxies might form.

It is possible that major spiral-spiral mergers can end up as even bigger spirals when the angular momentum vectors are in close alignment. Such alignment may occur naturally for spiral galaxies formed out of the same intergalactic filament. Simulations that collide two gas-rich disk galaxies in a prograde orbit are able to produce post-merger spiral galaxies, albeit at smaller scale (Barnes 2002; Springel & Hernquist

2005; Robertson et al. 2006). Because the dynamical timescales are longer for super spiral mergers, and their gaseous disks are highly dissipative, they may settle down into disks even when the angular momenta are not closely aligned.

Once a galaxy reaches the size of a super spiral, it is exceedingly unlikely that it will encounter another galaxy of similar size. That means that most of its interactions with other galaxies will be minor mergers. This can be visualized by looking again at Figure 7. There are at least 22 galaxies in the vicinity of 2MASX J11535621+4923562 that may merge with it and provide a continuous source of mass and gas for star formation. Even if the previously mentioned second-brightest cluster spiral were to collide and merge with this super spiral, the super spiral might survive with its disk intact.

It appears that the super spirals in our sample have so far avoided the fate of the vast majority of the most massive galaxies, and continue to form stars in spite of their extreme mass, bucking the trend of cosmic downsizing. There are several possible reasons for this success. First, super spirals may be robust to mergers because of their massive, dissipative gaseous disks. It appears that several super spirals in our sample have survived recent major mergers with their star-forming disks intact. Second, the supermassive black holes in super spiral bulges may not be large enough to provide enough feedback to drive away the gas in the giant galaxy disk. Third, the halo mass may not be large enough to cut off cold accretion onto the disk via accretion shocks. Finally, a large enough gas reservoir may have already settled into the disk to fuel star formation for a long time into the future.

7.3. Connection to Quenched Disk Galaxies

Super spirals occupy a relatively empty corner of the SFR vs. stellar mass diagram (Figure 1b). They lie above an extrapolation of the star forming main sequence, at the most extreme mass and SFR. We find that most super spirals have $\text{SSFR} > 0.08 \text{ Gyr}^{-1}$. They are forming stars at a rate that would allow them to build up their mass in less than the age of the universe. This is unlike similarly massive, yet much more common disk galaxies that fall below the star forming main sequence, in what we shall call the disk quenching sequence (DQS: the disk galaxy subset of the green valley population). The disk-quenching sequence is discussed in the context of SSFR and UV color evolution by Schawinski et al. (2014), and in the context of IR color evolution by Alatalo et al. (2014). Quenching disk galaxies are likely greatly reduced in their ability to form stars because their supply of cold gas has been cut off (e.g. Dekel & Birnboim 2006).

The most densely populated ridge of the DQS is close to the median stellar mass of our super spiral sample ($M_{\text{stars}} = 1.1 \times 10^{11} M_\odot$). We suggest that the majority of disk galaxies along this ridge were once super spirals. At a minimum, galaxies of this mass must have attained an average SFR $> 7 M_\odot \text{ yr}^{-1}$ in order to have formed in less than the age of the universe. This would put them squarely in the SFR and SSFR range of super spirals. A further implication is that their $D = 50 - 100 \text{ kpc}$ diameter stellar disks must have faded dramatically. If fossil giant disks are detected around massive lenticular galaxies with deep imaging, it will provide strong evidence

for this hypothesis. In addition, deep H I observations may reveal if their cold gas reservoir has been entirely depleted or reduced to a level that is not conducive to star formation.

8. CONCLUSIONS

We report the discovery of a large sample of the most luminous, biggest, and most massive spiral galaxies in the universe, which we call super spirals. These galaxies are very rare ($\sim 32 \text{ Gpc}^{-3}$), but are easily observed out to $z = 0.3$ because of their high luminosities and gigantic sizes. Super spirals are forming stars at $5\text{--}65 M_{\odot} \text{ yr}^{-1}$, a rate greater than their mean star formation rate over the age of the universe. Roughly 11% of super spirals have Seyfert or QSO nuclei, suggesting that they are still actively adding mass to their supermassive black holes. We find evidence that several super spirals are undergoing major mergers, but manage to keep their star-forming disks intact, and avoid being transformed into red-and-dead elliptical galaxies. Some super spirals are brightest cluster galaxies, while others appear to be isolated in the field. We suggest that super spirals may be the progenitors of red and dead lenticular galaxies of similar mass.

This work was made possible by the NASA/IPAC Extragalactic Database and the NASA/IPAC Infrared Science Archive, which are both operated by the Jet Propulsion Laboratory, California Institute of Technology, under contract with the National Aeronautics and Space Administration. We thank Joe Mazzarella, Ben Chan, Marion Schmitz, and the rest of the NED team for useful discussions and their support of this work. This publication makes use of data from the Galaxy Evolution Explorer, retrieved from the Mikulski Archive for Space Telescopes (MAST). STScI is operated by the Association of Universities for Research in Astronomy, Inc., under NASA contract NAS5-26555. Support for MAST for non-HST data is provided by the NASA Office of Space Science via grant NNX09AF08G and by other grants and contracts. Funding for the Sloan Digital Sky Survey IV has been provided by the Alfred P. Sloan Foundation, the U.S. Department of Energy Office of Science, and the Participating Institutions. SDSS-IV acknowledges support and resources from the Center for High-Performance Computing at the University of Utah. The SDSS web site is www.sdss.org. This publication makes use of data products from the Two Micron All Sky Survey, which is a joint project of the University of Massachusetts and the Infrared Processing and Analysis Center/California

Institute of Technology, funded by the National Aeronautics and Space Administration and the National Science Foundation. This publication makes use of data products from the Wide-field Infrared Survey Explorer, which is a joint project of the University of California, Los Angeles, and the Jet Propulsion Laboratory/California Institute of Technology, funded by the National Aeronautics and Space Administration. This work is based in part on observations made with the Spitzer Space Telescope, which is operated by the Jet Propulsion Laboratory, California Institute of Technology under a contract with NASA. We also make use of data from *Herschel*, an ESA space observatory with science instruments provided by European-led Principal Investigator consortia and with important participation from NASA. We thank Katey Alatalo for providing the SDSS-WISE comparison data in Figure 1a, which is adapted from Alatalo et al. (2014).

REFERENCES

- Alatalo, K., et al. 2014, *ApJL*, 794, 13
 Baldry, I. K., Glazebrook, K., Brinkmann, J. et al. 2004, *ApJ*, 600, 681
 Barnes, J. 2002, *MNRAS*, 333, 481
 Barnes, J. E. & Hernquist, L. E. 1991, *ApJL*, 370, 65
 Blanton, M. R. 2003, *ApJ*, 592, 819
 Bothun, G. D., Impey, C. D., Malin, D. F., & Mould, J. R. 1987, *AJ*, 94, 23
 Chang et al. 2015, *ApJS*, 219, 8
 da Cunha, E., Charlot, S., & Elbaz, D. 2008, *MNRAS*, 339, 1595
 Dekel, K. & Birnboim, Y. 2006, *MNRAS*, 368, 2
 Hopkins, P. F., Hernquist, L., Cox, T. J., Di Matteo, T., Robertson, B., & Springel, V. 2006, *ApJS*, 163, 1
 Joye, W. A., & Mandel, E. 2003, *ASPCs*, 295, 489, eds. Payne, H. E., Jedrezejewski, R. I. & Hook, R. N.
 Lilly, S. J., Carollo, C. M., Pipino, A., Renzini, A., & Peng, Y. 2013, *ApJ*, 772, 119
 Lintott, C. J. et al. 2008, *MNRAS*, 389, 1179
 Ogle, P. M. et al. 2015, *ASPCs*, 495, 25, eds. Taylor, A. R., & Rosolowsky, E.
 Ogle, P., Lanz, L., & Appleton, P. 2014, *ApJL*, 788, 33
 Robertson, B., Bullock, J. S., Cox, T. J. et al. 2006, *ApJ*, 645, 986
 Schawinski, K. et al. 2014, *MNRAS*, 440, 889
 Schechter, P. 1976, *ApJ*, 203, 297
 Sivanandam, S., Rieke, M. J., & Rieke, G. H. 2014, *ApJ*, 796, 89
 Snyder, G. et al. 2015, *MNRAS*, 454, 1886
 Springel, V., & Hernquist, L. 2005, *ApJL*, 622, 9
 Stoughton, C. et al. 2002, *AJ*, 123, 485
 Strateva, I., Ivezić, Z., Knapp, G. R. et al. 2001, *AJ*, 122, 1861
 Strauss, M. A., et al., *AJ*, 124, 1810
 Toomre, A. & Toomre, J. 1972, 178, 623
 Vogelsberger, M. et al. 2014, *MNRAS*, 444, 1518
 Wyder, T. K., et al. 2005, *ApJ*, 619, L15

Table 1
OGC Super Spiral Sample

SS	OGC	NED Name	$L(L_r^*)$	D^a	M_{stars}^b	SFR ^c	redshift ^d	NUV	r	u-r	Notes
01	0065	2MASX J10301576-0106068	13.9	81.3	11.25	1.54	0.28228	21.02 ^e	16.92	2.54	bar
02	0073	2MASX J10405643-0103584	13.4	82.2	11.39	0.97	0.25024	21.65	16.64	2.16	BCG
03	0139	2MASX J16394598+4609058	12.0	134.	11.05	1.48	0.24713	19.85	16.63	2.37	edge-on
04	0170	2MASX J10100707+3253295	11.6	87.1	11.27	1.40	0.28990	20.14	17.10	2.68	BCG, bar
05	0217	2MASX J13275756+3345291	11.2	68.8	11.05	1.81	0.24892	19.44	16.72	2.02	starburst, bar
06	0256	2MASX J11593546+1257080	10.9	87.2	10.89	1.26	0.26353	20.04	16.95	1.79	
07	0265	SDSS J115052.98+460448.1	10.8	88.1	10.94	< 0.74	0.28946	>21.51 ^e	17.19	3.25	faint spiral
08	0290	2MASX J12343099+5156295	10.6	62.4	11.13	1.71	0.29592	19.57	17.25	1.67	Sy1, asymm.
09	0299	2MASX J09094480+2226078	10.5	83.1	11.26	< 1.15	0.28539	21.40	17.25	3.73	BCG, shells?
10	0302	2MASX J15430777+1937522	10.5	65.5	11.37	2.45 ^f	0.22941	...	17.07	0.40	QSO, tidal arm
11	0306	SDSS J122100.48+482729.1	10.5	75.0	10.82	1.02	0.29966	20.15	17.29	1.69	
12	0345	2MASX J09260805+2405242	10.3	81.2	11.27	1.38	0.22239	19.61	16.57	3.38	BCG, face-on
13	0388	2MASX J17340613+6029190	10.1	63.5	11.20	1.27	0.27596	20.51	17.19	2.71	BGG
14	0441	SDSS J095727.02+083501.7	9.9	87.6	11.53	1.13	0.25652	20.88	16.99	2.19	
15	0454	2MASXi J1003568+382901	9.9	56.4	10.82	1.65	0.25860	19.79	16.97	1.70	starburst
16	0543	2MASX J09470010+2540462	9.6	99.3	11.07	1.13	0.10904	17.74	14.83	2.57	bar, Sy1?
17	0586	2MASX J11535621+4923562	9.5	90.2	11.11	1.43	0.16673	19.92	15.90	2.64	BCG, Sy2
18	0595	2MASX J07550424+1353261	9.5	76.6	11.12	1.30	0.22264	19.71	16.67	2.47	bar
19	0696	SDSS J102154.85+072415.5	9.2	69.7	< 11.57	1.35	0.29061	19.89	17.37	2.01	
20	0713	2MASX J08265512+1811476	9.2	81.9	11.27	1.32	0.26545	21.01	17.16	3.26	bar
21	0755	SDSS J113800.88+521303.9	9.1	63.9	10.76	1.14	0.29593	20.94	17.41	2.12	ring
22	0789	2MASX J08542169+0449308	9.0	86.0	10.96	1.30	0.15679	18.68	15.83	2.49	2 spirals, bar
23	0799	2MASX J10472505+2309174	9.0	72.2	11.12	1.20	0.18256	20.61	16.19	2.68	bar
24	0800	2MASX J11191739+1419465	9.0	70.8	10.93	1.15	0.14377	18.75	15.57	2.39	
25	0804	SDSS J135546.07+025455.8	9.0	84.2	< 11.35	1.01	0.23884	19.77	16.87	1.74	
26	0830	SDSS J141754.96+270434.4	9.0	68.6	10.70	1.11	0.15753	19.74	15.79	2.86	
27	0926	2MASX J10304263+0418219	8.8	72.7	11.19	1.60	0.16902	19.08	15.93	2.16	
28	0928	2MASX J12374668+4812273	8.8	66.0	11.01	1.57	0.27245	19.79	17.24	2.10	
29	0975	2MASX J11410001+3848078	8.7	72.1	11.08	1.38	0.26770	20.79	17.21	2.15	
30	0983	SDSS J153618.97+452246.8	8.7	80.2	10.48	1.07	0.23618	20.15	16.85	2.13	
31	1046	2MASX J09362208+3906291	8.6	69.6	10.99	1.37	0.28293	20.09	17.36	1.78	
32	1088	SDSS J140138.37+263527.6	8.5	78.2	< 11.50	1.24	0.28396	19.99	17.38	2.08	
33	1196	SDSS J154950.91+234444.1	8.4	69.3	< 11.35	1.30	0.26208	20.48	17.27	2.02	
34	1250	2MASX J12321515+1021195	8.3	71.4	10.95	1.06	0.16588	19.69	16.04	2.76	2 bulges?
35	1268	2MASX J12005393+4800076	8.3	62.7	11.10	1.45	0.27841	20.04	17.37	2.05	BCG
36	1273	2MASX J07380615+2823592	8.3	76.6	11.01	1.28	0.23091	20.13	16.92	2.34	
37	1304	2MASX J16014061+2718161	8.3	82.3	11.03	1.17	0.16440	17.60	16.06	1.60	BCG, 2 spirals
38	1312	SDSS J143447.86+020228.6	8.2	75.4	10.67	1.48	0.27991	20.43	17.42	2.24	
39	1323	SDSS J112928.74+025549.9	8.2	69.7	10.63	1.23	0.23960	19.56	17.01	2.00	
40	1352	SDSS J101603.97+303747.9	8.2	68.8	10.73	...	0.25191	21.16	17.13	2.94	
41	1375	2MASX J00155012-1002427	8.2	68.4	10.94	0.91	0.17601	...	16.23	2.09	
42	1395	2MASX J13103930+2235023	8.1	65.6	11.08	1.15	0.23123	19.91	16.87	2.59	
43	1420	2MASX J13475962+3227100	8.1	87.5	10.94	1.23	0.22306	20.25	16.79	2.37	BGG
44	1464	2MASX J10041606+2958441	8.1	57.4	11.04	1.81	0.29844	20.64	17.59	2.06	starburst
45	1500	2MASX J10095635+2611324	8.1	63.7	10.98	1.33	0.24089	19.99	17.03	2.19	
46	1501	2MASX J09334777+2114362	8.1	63.6	11.00	1.69	0.17219	17.84	16.17	1.60	QSO, 2 nuclei
47	1544	2MASX J14472834+5908314	8.0	68.4	11.13	1.13	0.24551	20.22	17.04	2.15	
48	1546	2MASX J13435549+2440484	8.0	60.7	11.05	0.89	0.13725	19.54	15.56	2.50	
49	1554	2MASX J13422833+1157345	8.0	57.1	11.08	1.43	0.27873	21.66	17.43	2.20	
50	1559	CGCG 122-067	8.0	81.4	11.13	1.00	0.08902	18.27	14.56	3.13	BCG, 2 bulges
51	1606	SDSS J121644.34+122450.5	8.0	77.9	< 11.31	1.13	0.25694	20.12	17.22	1.76	bar, Sy1
52	1608	SDSS J040422.91-054134.9	8.0	79.5	10.56	1.07	0.25055	20.38	17.27	2.37	flocculent
53	1611	2MASX J00380781-0109365	8.0	83.9	11.31	0.91	0.20828	21.33	16.65	4.38	E with shells?

^a Isophotal diameter (kpc) at $r = 25.0$ mag arcsec⁻².

^b $\log_{10} M_{stars} (M_{\odot})$ or 3σ upper limit, based on 2MASS Ks luminosity and u-r color.

^c $\log_{10} \text{SFR} (M_{\odot} \text{ yr}^{-1})$ or 95% confidence upper limit, based on WISE [12] luminosity.

^d SDSS DR9 redshift.

^e GALEX photometry measured in 14'' aperture. Source not in GASC or GMSC.

^f This SFR may be overestimated by a large factor because of the QSO nucleus.

^g WISE data compromised by nearby IR-bright star.

Table 2
Candidate Cluster and Group Membership

SS	NED Name	redshift	N1 ^a	N10 ^b	Cluster Name	type	redshift	ztype	sep(')
2	2MASX J10405643-0103584	0.250303	1	8	SDSS CE J160.241898-01.069106	GClstr	0.254019	EST	0.013
4	2MASX J10100707+3253295	0.289913	2	17	GMBCG J152.52936+32.89139	GClstr	0.319000	PHOT	0.001
9	2MASX J09094480+2226078	0.285386	1	9	GMBCG J137.43670+22.43538	GClstr	0.303000	PHOT	0.000
12	2MASX J09260805+2405242	0.222451	1	22	WHL J092608.1+240524	GClstr	0.178000	PHOT	0.000
13	2MASX J17340613+6029190	0.275807	1	2	SDSSCGB 59704	GGroup	0.276000	SPEC	0.450
17	2MASX J11535621+4923562	0.166892	3	69	OGC 0586 CLUSTER	GClstr
35	2MASX J12005393+4800076	0.278617	1	13	GMBCG J180.22479+48.00211	GClstr	0.252000	PHOT	0.001
37	2MASX J16014061+2718161	0.164554	3	163	GMBCG J240.41924+27.30444	GClstr	0.193000	PHOT	0.000
43	2MASX J13475962+3227100	0.223113	1	13	SDSSCGB 16827	GGroup	0.748
50	CGCG 122-067	0.089008	5	302	MSPM 05544	GClstr	0.089190	SPEC	0.001

^a Number of galaxies within 1 Mpc and 500 km s⁻¹.

^b Number of galaxies within 10 Mpc and 5000 km s⁻¹.

APPENDIX

CUSTOM PHOTOMETRY AND VALIDATION OF M_{STARS} AND SFR

In order to validate our stellar mass and SFR estimates, which are based on Ks, u, r, WISE [12], and [22] μ m photometry, we make a more detailed analysis of two representative examples from our super spiral sample. We remeasure their photometry in matched apertures, rather than relying on catalog photometry. Then we fit their SEDs to make full use of the available multi-band photometry to estimate more accurate M_{stars} and SFR. We chose SDSS J094700.08+254045.7 for this analysis because it is one of the brightest super spirals in our sample, with good photometry in many bands, and typical colors. The SDSS spectrum of its bulge is also typical of most super spirals, being dominated by an old stellar population (Figure A1). We also make a detailed study of 2MASX J13275756+3345291, which is the most luminous mid-IR source in our sample and has an SDSS nuclear spectrum with strong young stellar component and high-equivalent width H α emission (Figure A2), characteristic of starburst activity.

We remeasured GALEX (FUV, NUV), SDSS (u, g, r, i, z), 2MASS (J, H, Ks) and WISE band 1-4 photometry for SDSS J094700.08+254045.7 using the SAOImager ds9 (Joye & Mandel 2003) on images retrieved from MAST, SDSS, and IRSA (Figure A3). Aperture and color corrections were applied as necessary and the GALEX and SDSS photometry was corrected for foreground extinction due to the Milky Way dust (Wyder et al. 2005; Stoughton et al. 2002). The Galactic extinction is a modest $A_V = 0.063$ mag (NED). We used an elliptical aperture with semi-major and semi-minor axes of 31''5 and 25''5, respectively, in order to capture the full flux of the spiral disk in all bands. This corresponds to major and minor diameters of 125 kpc and 102 kpc. We also compute 3σ IRAS upper limits based on the RMS uncertainty measured by IRSA's Scan Processing and Integration tool (SCANPI) to constrain the FIR luminosity.

We present the SED of SDSS J094700.08+254045.7 in Figure A4. The galaxy is detected in all GALEX, SDSS, 2MASS, and WISE bands, but is undetected by IRAS. The UV through near-IR data points reveal a massive old stellar population plus a young stellar population. Mid-IR emission appears to be dominated by PAHs and warm dust from star formation. We fit the SED using MAGPHYS template fitting (da Cunha, Charlot, & Elbaz 2008). This gives a total stellar mass of $1.8_{-0.3}^{+0.3} \times 10^{11} M_\odot$ and a star formation rate of $9.9_{-0.3}^{+1.6} M_\odot \text{ yr}^{-1}$. We get a consistent estimate of $1.2 \pm 0.1 \times 10^{11} M_\odot$ for the stellar mass from the u-r color and K band luminosity, applying the Bell et al. (2003) prescription for color-dependent mass-to-light ratio (Table 1). The WISE band 3 luminosity gives a consistent star formation rate of $13.5 \pm 0.2 M_\odot \text{ yr}^{-1}$, using the prescription of Chang et al. (2015). Lacking FIR detections, we do not have a good handle on the total dust mass, however, the SED fit formally yields a dust mass of $\sim 10^8 M_\odot$, based on the PAH emission and FIR upper limits. This corresponds to roughly $\sim 10^{10} M_\odot$ of gas, assuming a standard gas/dust ratio of 100.

We remeasured GALEX (FUV, NUV), SDSS (u, g, r, i, z), 2MASS (J, H, Ks) and WISE band 1-4 photometry for 2MASX J13275756+3345291 (Figure A5), using a similar procedure. We also retrieved Spitzer IRAC and MIPS, and Herschel PACS and SPIRE images from the respective IRSA and ESA archives to measure the IR fluxes. We used a circular aperture with 20''0 (156 kpc) radius for most bands. However, at SPIRE wavelengths, we used the larger point source apertures of 22'', 30'', and 42'', in order to contain the broader PSF. The Galactic extinction is only $A_V = 0.034$ mag (NED).

We present the SED in Figure A6. The galaxy is detected in all measured bands except the SPIRE 500 μ m band. In contrast to SDSS J094700.08+254045.7, there is a stronger component of emission from young stars, and much more luminous IR emission from star formation activity. We fit the SED using MAGPHYS, yielding a total stellar mass of $2.04_{-0.09}^{+0.05} \times 10^{11} M_\odot$ and a star formation rate of $40.5_{-0.5}^{+6.5} M_\odot \text{ yr}^{-1}$. The stellar mass is consistent with the value of $1.6 \pm 0.3 \times 10^{11} M_\odot$ that we obtain from the u-r color and K band luminosity (Table 1). The WISE [12] luminosity gives a somewhat larger star formation rate of $65 \pm 4 M_\odot \text{ yr}^{-1}$, using the conversion factor of Chang et al. (2015). The

Herschel FIR measurements yield a secure estimate of total dust mass from the SED fit of $7_{-1}^{+3} \times 10^8 M_{\odot}$, corresponding to $7 \times 10^{10} M_{\odot}$ of gas, assuming a standard gas/dust ratio of 100.

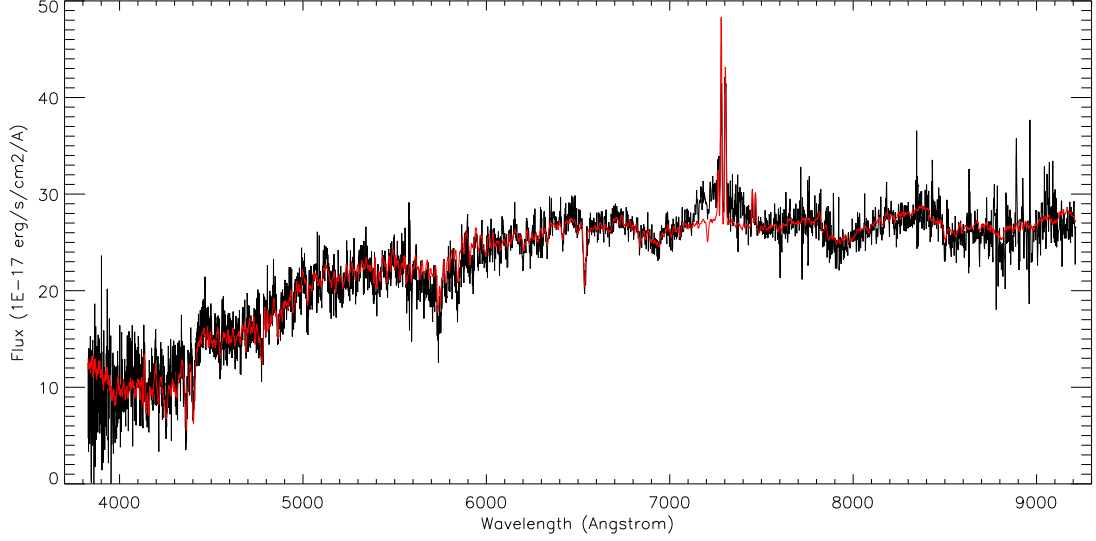


Figure A1. SDSS DR9 optical spectrum and spectral model of SDSS J094700.08+254045.7. Note the possible broad H α emission line not fit by the spectral model, indicative of a Seyfert 1 AGN.

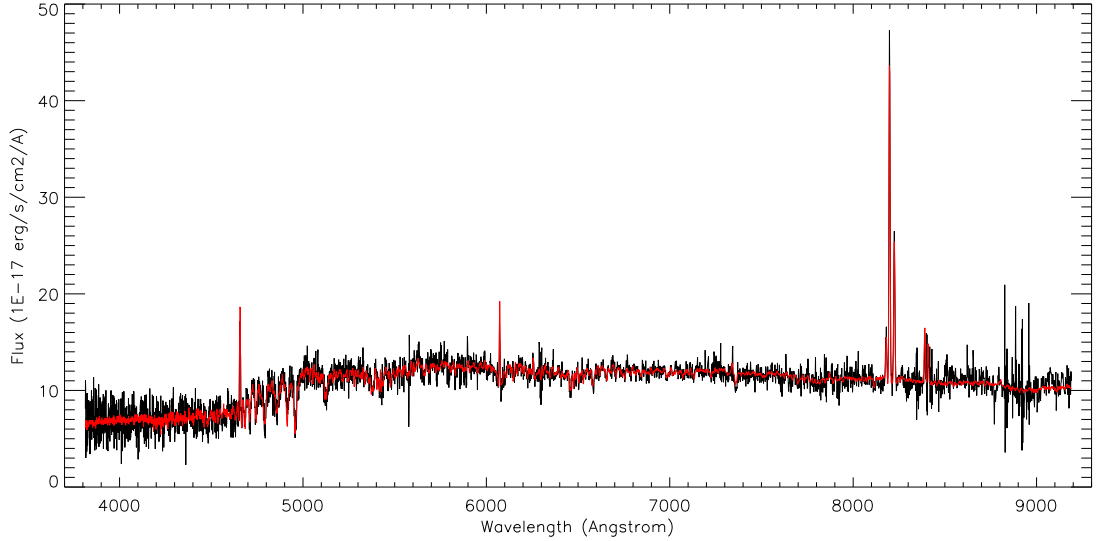


Figure A2. SDSS DR9 optical spectrum and spectral model of 2MASX J13275756+334529. The blue spectral slope and strong H α emission indicate starburst activity in the galaxy bulge, consistent with the high star formation rate in the galaxy as a whole.

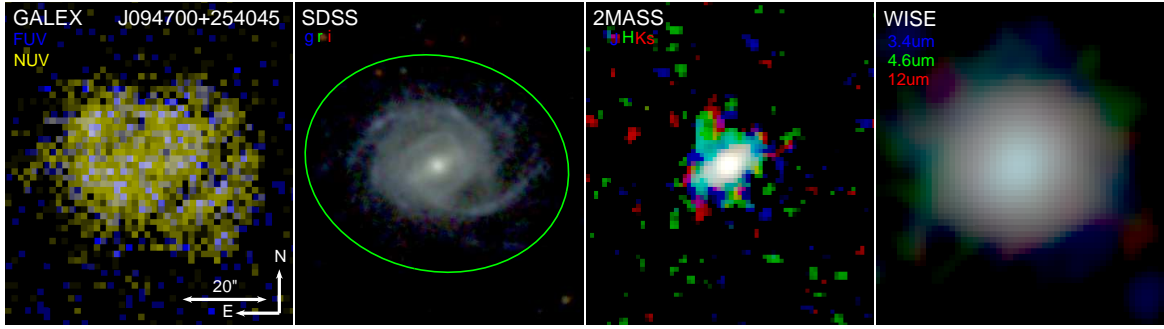


Figure A3. GALEX, SDSS, 2MASS and WISE images of SDSS J094700.08+254045.7. The image scale is $1.991 \text{ kpc}''$. The photometric aperture with major and minor axes of 125 kpc and 102 kpc, respectively, is indicated by the ellipse on the SDSS image.

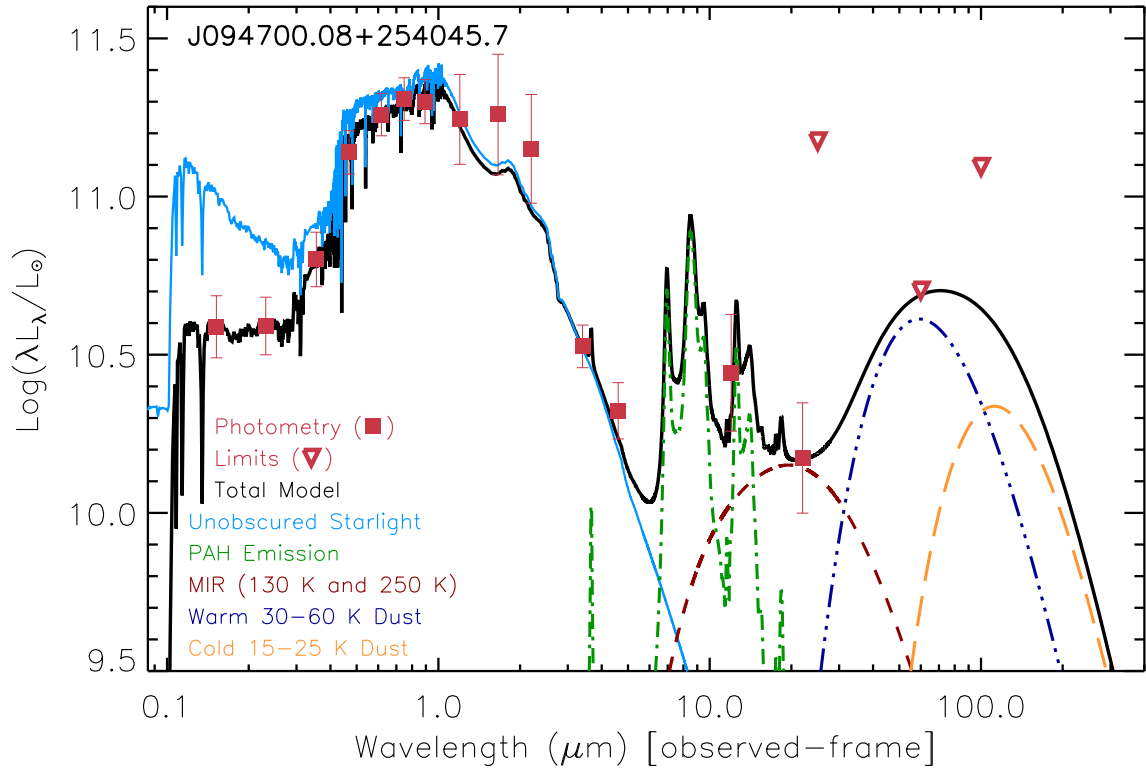


Figure A4. Spectral Energy Distribution of SDSS J094700.08+254045.7 fit by MAGPHYS. GALEX (NUV, FUV), SDSS (u, g, r, i, z), 2MASS (J, H, Ks), and WISE band 1-4 photometry are measured in the aperture shown in Figure A3. IRAS upper limits at 25, 60, and $100 \mu\text{m}$ are estimated using SCANPI.

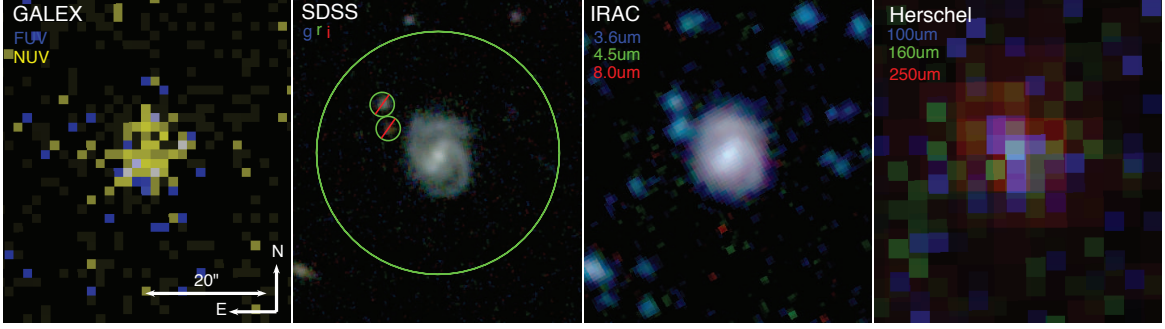


Figure A5. GALEX, SDSS, IRAC, and *Herschel* images of 2MASX J13275756+334529. The image scale is $3.898 \text{ kpc}''$. The circular photometric aperture with diameter 156 kpc and two exclusion regions are indicated on the SDSS image.

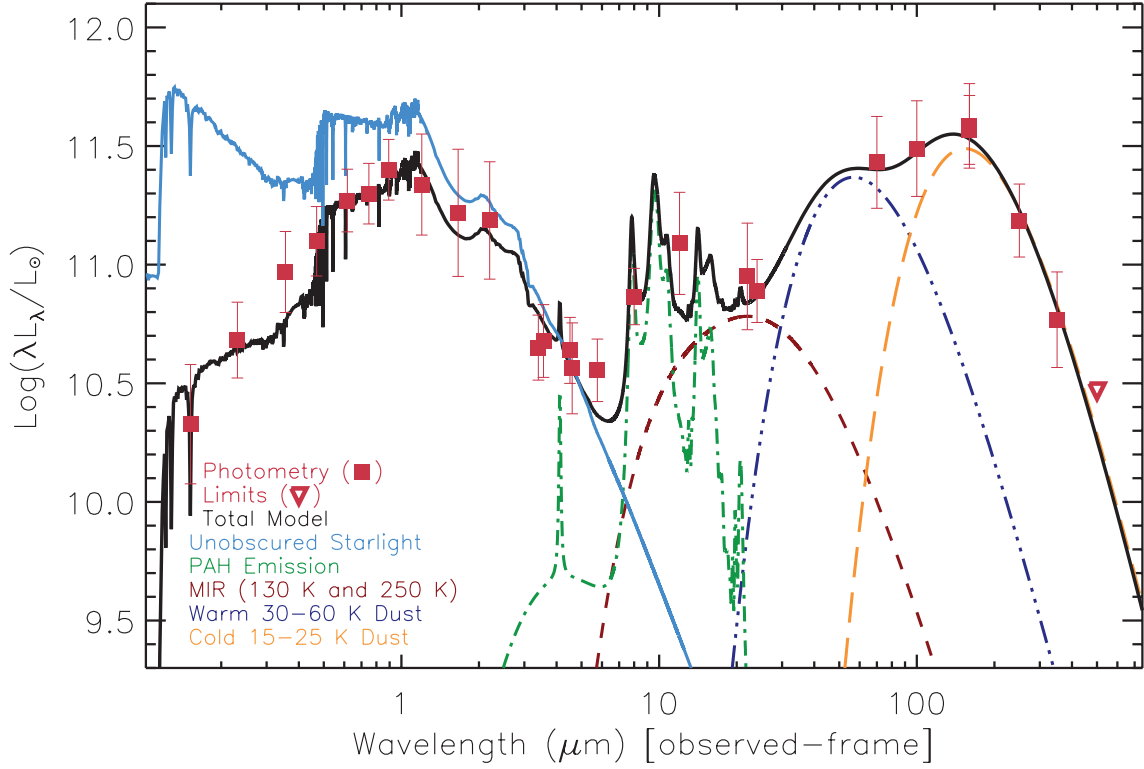


Figure A6. Spectral Energy Distribution of 2MASX J13275756+334529 fit by MAGPHYS. GALEX (NUV, FUV), SDSS (u, g, r, i, z), 2MASS (J, H, Ks), Spitzer IRAC and MIPS 24, 70, and $160 \mu\text{m}$, WISE band 1-4, *Herschel* PACS 100 and $160 \mu\text{m}$, and SPIRE photometry are measured in the aperture shown in Figure A5. SPIRE $500 \mu\text{m}$ luminosity is an upper limit.